

Radial velocities of pulsating subdwarf B stars: KPD 2109+4401 and PB 8783 \star

C. Simon Jeffery¹ and Don Pollacco^{2,3}

¹*Armagh Observatory, College Hill, Armagh BT61 9DG, Northern Ireland*

²*Isaac Newton Group, La Palma*

³*Queens University Belfast, Belfast BT7 1NN, Northern Ireland*

Accepted . Received ;

ABSTRACT

High-speed spectroscopy of two pulsating subdwarf B stars, KPD 2109+4401 and PB 8783, is presented. Radial motions are detected with the same frequencies as reported from photometric observations and with amplitudes of $\sim 2 \text{ km s}^{-1}$ in two or more independent modes. These represent the first direct observations of surface motion due to multimode non-radial oscillations in subdwarf B stars. In the case of the sdB+F binary PB 8783, the velocities of both components are resolved; high-frequency oscillations are found only in the sdB star and not the F star. There also appears to be evidence for mutual motion of the binary components. If confirmed, it implies that the F-type companion is $\gtrsim 1.2$ times more massive than the sdB star, while the amplitude of the F star acceleration over 4 hours would constrain the orbital period to lie between 0.5 and 3.2d.

Key words: stars: individual: KPD 2109+4401, stars: individual: PB 8783, stars: oscillations, stars: variables: other (EC14026/sdBV)

1 INTRODUCTION

The discovery of small-amplitude non-radial pulsations in a number of subdwarf B stars (sdBVs) has introduced a powerful new tool for the study of stellar remnants (Kilkenny et al. 1997=SDBVI and subsequent papers). Long time-series photometric campaigns have detected rich spectra of oscillations in over a dozen targets, with frequencies and amplitudes generally indicative of low-order ($\ell = 0 - 2$) and low-degree modes. The discovery has revolutionized the study of subdwarf B stars for the simple reason that pulsations in these stars were not expected. From a theoretical point of view, it appears that the pulsation mechanism is only effective when diffusion processes modify the outer layers of the star. Metal-enrichment in a specific layer must conspire with the local temperature to drive pulsations through the opacity mechanism (Charpinet et al. 1997).

In terms of their effective temperature and surface gravity, sdBVs are indistinguishable from their non-variable counterparts – there is no instability strip in which all sdBs pulsate. The origin of all sdBs remains a puzzle, although the increasing detection of sdB binarity, including several sdBVs, may point to a previous phase of common-envelope

evolution in many, if not all. The structure of sdBs is partially hidden as a consequence of atmospheric diffusion, which disguises the true composition and the mass of the hydrogen-rich envelope, both of which are key diagnostics of previous evolution. By enabling an exploration of the composition and mass of these outer layers, asteroseismology may be of a pivotal importance.

Immediately after the discovery of sdBV pulsations, we recognized the potential for spectroscopy to provide additional diagnostics. Mode identification from photometry alone is challenging, and could be assisted by the identification of line-profile variations, whilst the comparison of radial and light amplitudes could be used to determine stellar radii directly. Spectroscopy might also demonstrate the presence of higher-order modes not detected photometrically. The limitations are that the periods are short (100-500s) compared with conventional CCD readout times, the stars are faint (12–15 mag.), and the photometric amplitudes are typically only a few tenths of one per cent. High-resolution high-S/N multi-line studies such as those obtained for non-radial oscillations in rapidly rotating bright O and B stars (e.g. Reid et al. 1993, Telting, Aerts & Mathias 1997) would not appear to be feasible. However, the development of new techniques offered the possibility to acquire high-speed spectroscopy of sdBVs and here we report our first successful observations obtained in 1998 October. Subsequently,

\star Based on observations obtained with the William Herschel Telescope, ING, La Palma, Spain

Table 1. Summary of 1998 October WHT driftmode observations of sdBVs

Star	Date	V	t (s)	c	s	j	Σn
PB 8783	1998 Oct 3	12.3	7.9	325	23	57	1400
KPD 2109 +4401	1998 Oct 4	13.4	9.8	230	14	57	1200

O’Toole et al. (2000) announced preliminary results of independent radial velocity observations. They report a 9 km s^{-1} amplitude periodic variation in the large amplitude sdBV PG1605+072 at the principal frequency of 2.10 mHz found photometrically by Koen et al. (1998, SDBV VII).

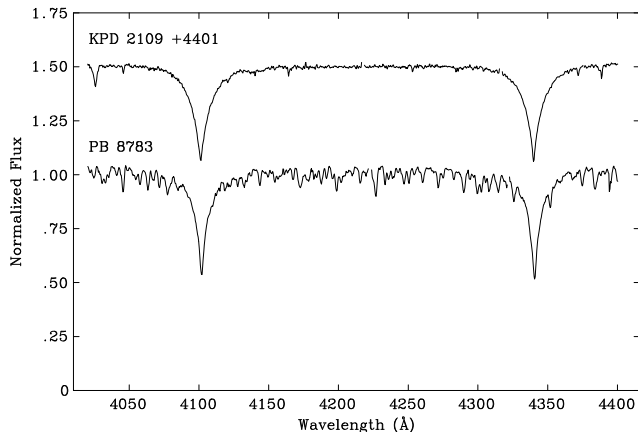
2 OBSERVATIONS

The targets selected for our initial study were PB 8783 (Koen et al. 1997 = SDBV II) and KPD 2109+4401 (Koen et al. 1998 = SDBV XI, Billères et al. 1998). Although not ideal, our observations were scheduled when possibly more exciting targets such as PG1336–018 (Kilkenny et al. 1998 = SDBV VIII) and PG1605+072 (SDBV VII) were not accessible. On the other hand, both targets have been well-studied photometrically (O’Donoghue et al 1998 = SDBV V, SDBV XI, Billères et al. 1998) and show multiple periods in the ranges 7–10 and 5–6 mHz respectively, with amplitudes of a few millimagnitudes.

Observations were obtained with the 4.2m William Herschel Telescope on 1998 October 3 and 4 using the blue arm of the intermediate dispersion spectrograph ISIS. The R1200B grating and the TEK1 CCD with 1124^2 $24\mu\text{m}$ pixels yielded an instrumental resolution (2 pixel) $R = 5000$ in the wavelength interval 4020–4420 Å. This wavelength region was chosen because it contains two strong Balmer lines and, potentially, a number of neutral helium and minor species lines that are normally observed in early-B stars. It also maximises the photon collection rate.

The CCD was read out in low-smear drift mode (Rutten et al. 1997), in which only a small number j of CCD rows (parallel to the dispersion direction) are read out at one time. A dekker is used to limit the slit-length, thus only a fraction of the CCD window, $\simeq j$ rows, is exposed at one time. After exposing for an interval t , the CCD contents are stepped down by j rows. This charge transfer imposes a small dead time d which is roughly proportional to the CCD window size. Each set of j rows is accumulated into a data cube containing n individual 2D spectra, stacked adjacent to one another. In practice the first few spectra in the frame are null, corresponding to the unexposed part of the CCD being read out before exposed rows reach the CCD edge. Comparison lamps and stellar spectra can be obtained in exactly the same way. Maximum frame sizes limit n to a few hundred; we normally adopted $n = 200$ before beginning a new frame.

In our experiment, j was set just wide enough to admit a small region of sky either side of the stellar image and to allow for edge effects between adjacent spectra. On-chip binning by a factor of 3 further reduced the read-out time and data-volume. t was chosen so that $t + d$ was approxi-

**Figure 1.** The mean spectrum obtained for each of two pulsating sdB stars observed in 1998 October. See text for further details.

mately $1/10$ of the typical observed pulsation period. Values for t , j and Σn are given for each target in Table 1, together with the average number of counts detected per wavelength resolution element c , and the maximum S/N ratio s anticipated in each exposure from nominal performance figures (SIGNAL, Benn 1997). In this configuration, $d = 1.57\text{s}$ and the read-out noise was 5.24 electrons per pixel.

Due to occasional errors in the CCD controller, not all exposure times t were equal, roughly one in 100 exposures would drop by an unpredictable amount. These were identified by integrating the total counts in each individual spectrum and adjusting individual exposure times to reflect the photometry.

The data cubes were reduced using scripted standard IRAF routines. After bias subtraction and flatfielding, the 1-dimensional spectra were optimally extracted and sky subtracted. The copper-argon arc spectra obtained at the beginning and end of each data cube were time weighted for each stellar observation and the corrected calibration derived and applied. Over the duty cycle of one data cube the arc shifts were never greater than a few microns. Further reductions included normalization of the spectra and cosmic ray removal.

Cross-correlation of the arc spectra showed that the maximum shift during a half hour period was around 7 microns (about a quarter of a pixel). Arc exposures showed that this was varying smoothly during the night and as calibration data were obtained before and after each stellar data cube, then simple spectral interpolation of the extracted one dimensional spectra (weighted by the time interval from the bracketing arc spectra) removed any instrumental shift to probably within 1 micron ($< 0.9 \text{ km s}^{-1}$).

The final data product is a set of files each containing n 1-dimensional wavelength-calibrated flux-normalized spectra. Each spectrum is time-tagged. The mean spectrum for each of our targets is shown in Fig. 1

3 ANALYSIS AND RESULTS

The primary objective of our observations was to detect and measure radial motion due to the dominant oscillatory modes detected from photometry. There was the ad-

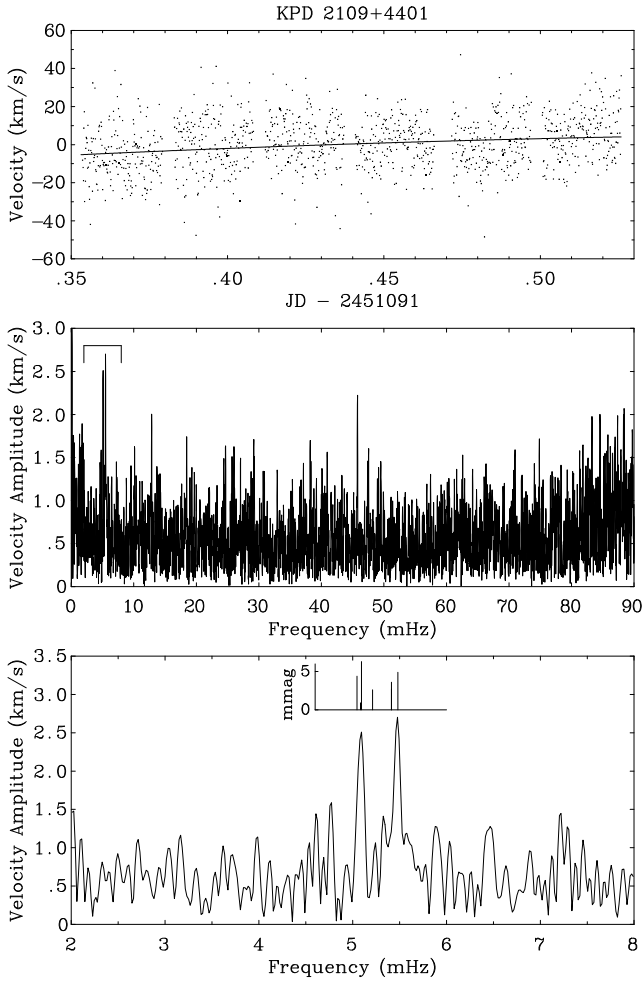


Figure 2. Radial velocities and amplitude spectrum of KPD 2109+4401 from WHT high-speed spectroscopy on 1998 Oct 4. The slowly varying function $b(t)$ is shown in the top panel. The bottom panel is an enlargement of the marked section of the amplitude spectrum shown in the middle panel. The amplitudes of photometric frequencies inset in the bottom panel are taken from SDBV IX.

ditional possibility that line-profile variations or multiple modes might be detected, as well as any mutual motion within any binary system.

The most commonly adopted method for measuring radial-velocity shifts in stellar spectra is the cross-correlation function (ccf). We constructed a mean spectrum for each target. This template was cleaned to remove stationary features such as bad CCD columns. Both template and individual spectra were continuum-subtracted; they were already linearized to the same wavelength scales. The ccf for each spectrum relative to the template was computed and stored as a 2d function $\chi(t, v)$, where t is now time, δt is the mean sampling interval and v is radial velocity relative to the template. The velocity of each spectrum was found by a) fitting a gaussian to, b) fitting a parabola to and c) computing the centroid of $\chi(v)$ in the range $-\delta v$ to $+\delta v$, to give functions $v_g(t)$, $v_p(t)$, and $v_c(t)$, respectively. Moments $M_j(t) = \int (v - v_{\text{ref}})^j \chi(v, t) dv$; $j = 1, 2, 3$ were also computed. With $v_{\text{ref}} = 0$, M_1 corresponds to the centroid. $v(t)$

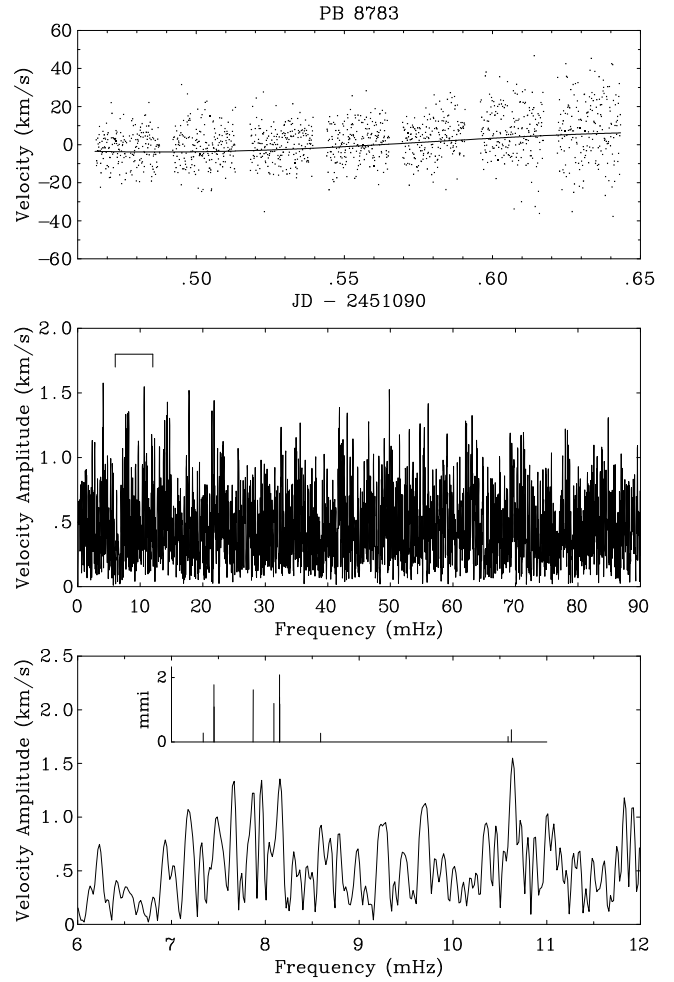


Figure 3. As Fig. 2 for PB 8783 (1998 Oct 3). The photometric frequencies are taken from SDBV V, mmi denotes parts-per-thousand and 1 mmi equals 1.086 mmag.

was sensitive both to the method chosen and the value of δv .

The functions $v(t)$ were investigated for periodic content by means of the discrete Fourier transform \mathcal{F} . Either a low-degree polynomial or a long-period sine function $b(t)$ was first fit and subtracted from $v(t)$. $\mathcal{F}\{v(t) - b(t)\}$ was then computed.

The velocity data $v_p(t)$ and \mathcal{F} are shown in Figs. 2 and 3. These figures also show a representation of the principal frequencies and amplitudes discovered photometrically \mathcal{P} (SDBV V, IX) [†].

The information we require from the amplitude spectrum is not in the first instance the significance of the peaks but rather the amplitude associated with expected frequencies. Over the entire range $0.1 \sim 2/\Sigma n \delta t < \nu/\text{mHz} < 1/\delta t \sim 90$, \mathcal{F} shows many peaks of comparable amplitude which on their own have little statistical significance. However the coincidence in Figs. 2 and 3 of the highest peaks in \mathcal{F} with the highest peaks in \mathcal{P} is more remarkable and is regarded as

[†] Throughout this paper, the term amplitude applied to periodic signals refers to the semi-amplitude a of the sine function $a \sin(2\pi\nu t + \phi)$

Table 2. Velocity amplitudes of detected pulsation modes in KPS 2109+4401. ν_p is the photometric frequency, a_p the photometric amplitude (SDBV IX), ν_v the frequency of the measured velocity peak, a_v the measured velocity amplitude.

ν_p mHz	a_p mmag	ν_v mHz	a_v km s^{-1}
5.0455	4.4]		
5.0842	0.9	5.09	2.49
5.0939	6.3]		
5.2124	2.6		
5.4127	3.6]		
5.4136	2.7	5.48	2.68
5.4818	4.9]		

Table 3. Simulated multifrequency observations: ν, a are the frequencies and amplitudes of the test signal, n is the number of test runs, σ is the standard deviation of normally-distributed noise. a' are the mean and variance of the highest detected signal within ± 0.1 mHz of the principal test frequencies.

ν mHz	a km s^{-1}	n	σ km s^{-1}	$\langle a' \rangle$ km s^{-1}	a/a'
KPD 2109+4401 6 frequency simulation					
5.050	2.20]	100	15		
5.080	0.45				
5.090	3.15]			3.23 ± 0.76	0.98 ± 0.23
5.410	1.80]				
5.480	2.45]			2.71 ± 0.27	1.06 ± 0.08
5.210	1.30			1.84 ± 0.18	0.71 ± 0.10
KPD 2109+4401 low-noise simulation					
5.050	2.20]	30	0		
5.080	0.45				
5.090	3.15]			3.47 ± 0.91	0.91 ± 0.26
5.410	1.80]				
5.480	2.45]			2.53 ± 0.10	0.97 ± 0.04
5.210	1.30			1.48 ± 0.05	0.88 ± 0.04
KPD 2109+4401 2 frequency simulation					
5.090	3.15	100	15	3.09 ± 0.31	1.02 ± 0.10
5.480	2.45			2.38 ± 0.39	1.03 ± 0.16
PB 8783 5 frequency simulation					
7.340	1.30	100	15	1.54 ± 0.17	0.84 ± 0.11
7.456	1.80			1.96 ± 0.30	0.92 ± 0.15
7.862	1.40			1.71 ± 0.22	0.82 ± 0.13
8.140	2.40			2.35 ± 0.27	1.02 ± 0.12
10.619	2.60			2.48 ± 0.31	1.05 ± 0.13

a positive signature of oscillatory behaviour in the spectroscopic data. The resolution $2/n\delta t \sim 0.1\text{mHz}$ in \mathcal{F} is insufficient to resolve the fine structure observed in much longer photometric time series.

3.1 KPD 2109+4401

Because its spectrum is not contaminated by that of a late-type companion, the results for KPD 2109+4401 are the less complicated to interpret. A background drift of approximately 9km s^{-1} over 5 hours is approximately linear and defines b . We adopted $\delta v = 150\text{km s}^{-1}$ to establish $v_p(t)$

and to construct Fig. 2. Principal peaks in the amplitude spectrum are evident at $\nu_1 = 5.09\text{mHz}$ and $\nu_2 = 5.48\text{mHz}$.

The same frequency structure in \mathcal{F} was obtained for $\delta v = 150, 300$ and 450km s^{-1} when either a gaussian, parabolic fit or centroid is used to measure $v(t)$. In the interval 4.5–6.4 mHz, minor peaks occurred at $\nu_{3-7} = 4.77, 5.24, 5.33, 5.90$ and 6.03mHz in most of these analyses. Beating may be responsible for some peaks; for example $\nu_3 = \nu_1 - (\nu_2 - \nu_1), \nu_6 = \nu_2 + (\nu_2 - \nu_1)$. Thus only ν_1 and ν_2 could be identified as genuine from the present data.

The probability of finding a set of peaks at prespecified frequencies and exceeding a given amplitude threshold by chance may be computed as follows. For a given frequency range Δv , count the number of peaks n which exceed a given threshold v_{thresh} . Then count the number of peaks n_{id} which lie within a resolution width $\pm\delta v$ of the predicted frequencies. The probability of this number occurring by chance is

$$p = \left(n \frac{2\delta v}{\Delta v} \right)^{n_{\text{id}}}.$$

For KPD 2109+4401, we chose $\Delta v = 6\text{mHz}$, $v_{\text{thresh}} = 1.5\text{km s}^{-1}$ and $\delta v = 0.05\text{mHz}$ which gave $n = 3$, $n_{\text{id}} = 2$ and hence $p = 0.0025$.

In order to interpret the amplitudes of the identified peaks, we carried out the following numerical experiment (table 3). We first formed the sum of a series of sine functions each having a frequency ν_i , amplitude a_i and a random phase shift ϕ_i . The ν_i and a_i were based on the photometric results for KPD 2109+4401 (SDBV IX). This sum was sampled at the same times t_j as the observations,

$$s(t_j) = \sum_i a_i \sin(2\pi\nu_i t_j + \phi_i).$$

To this we added normally-distributed noise with a standard deviation $\sigma = 15\text{km s}^{-1}$ similar to the observational scatter. \mathcal{F} was derived and usually found to contain peaks at the principal input frequencies, but not always with the same amplitude ratios. Minor peaks were less frequently identified. The amplitudes of the highest peaks within $\pm 0.1\text{mHz}$ of the test frequencies were measured. This procedure was repeated n times and the average amplitudes for each detected frequency $\langle a'_i \rangle$ were computed. In the case of KPD 2109+4401, the spacing of some input frequencies is less than the resolution provided by the limited time series. Consequently, the measured amplitudes represent some sum from several independent sine functions. Interference, or beating, means that the apparent amplitude of such a signal will vary according to the relative phases of the components. This is apparent in table 3 (six-frequency simulation), where the relative standard deviation of the amplitude of the composite signal at 5.09 mHz is much higher than that of the single-frequency signal at 5.21 mHz. The experiment was repeated with only two well-resolved input frequencies and yielded the ratio $a'/a \sim 1.0 \pm 0.1$. Reducing σ reduces the error on a'/a due to experimental noise, but not that due to mode beating or to data sampling. It was also repeated for ν and a appropriate to the second target PB 8783 with a similar result.

Therefore, we conclude that the peak amplitudes of 2.49 and 2.68km s^{-1} at frequencies 5.09 and 5.48 mHz in KPD 2109+4401 reflect to within $\sim 20\%$ (standard deviation) the combined real amplitudes of oscillations within $\sim 0.05\text{mHz}$ of these frequencies (Table 2). The principal

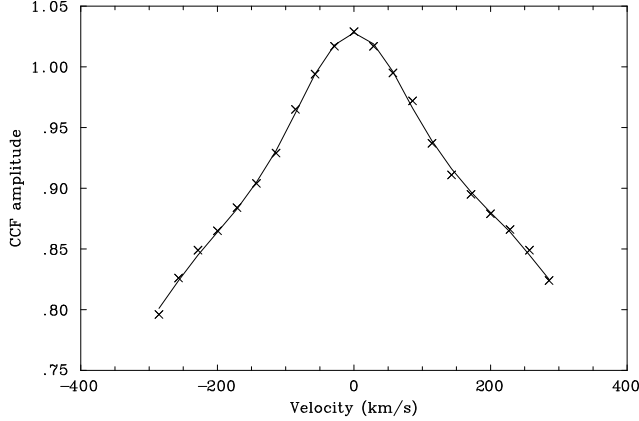


Figure 4. Peak of a typical cross-correlation function $\chi(v)$ for PB 8783 (crosses). The gaussian + quadratic fit used to construct the two-component velocity solution (Figs. 5 and 6) is also shown (solid line).

causes of uncertainty in the amplitudes are beating between unresolved modes and experimental noise.

The 9 km s^{-1} drift in b may be real. Instrumental drift is limited to $\lesssim 0.9 \text{ km s}^{-1}$ (section 2). The heliocentric correction, which was not applied to the data, changes by less than 0.4 km s^{-1} . In the simulations described above, the r.m.s. amplitude of b was 1.7 km s^{-1} . Although KPD 2109+4401 is not known to be a binary, it cannot be ruled out. PG 1336-018 was only recognised as a binary from its eclipses; the secondary is too faint to be detected spectroscopically (SDBV VIII).

3.2 Line profile variations?

In addition to radial-velocity information, χ contains information about line-profile variations, since the ccf represents an average line profile within the region of spectrum analyzed. In the present case, the average line profile is dominated by two Balmer lines, $H\gamma$ and $H\delta$. The average line width and asymmetry are indicated either by the moments $M_{2,3}$, respectively, or by the coefficients $g_{2,4}$ in the gaussian + linear fit $g(v) = g_0 \exp((v - g_1)^2/g_2) + g_3 + g_4v$.

Neither the Fourier transform $\mathcal{F}\{M_2(t)\}$ or $\mathcal{F}\{g_2(t)\}$ showed peaks near ν_1 or ν_2 . With suitably chosen δv , both $\mathcal{F}\{M_3(t)\}$ and $\mathcal{F}\{g_4(t)\}$ showed frequency structure similar to $\mathcal{F}\{v(t)\}$. However, the amplitude of peaks in $\mathcal{F}\{M_1(t)\}$ only approached that of $\mathcal{F}\{v_p(t)\}$ if δv was sufficiently large, in which case the periodic content of $M_3(t)$ was essentially lost. This implied that M_3 contained velocity information not properly incorporated into M_1 .

$\mathcal{F}\{g_4(t)\}$ showed peaks at 5.09 and 5.55 mHz with $\delta v \sim 400 - 600 \text{ km s}^{-1}$, but not otherwise. In the case of intrinsically sharp lines, such asymmetry may reflect differential radial motion across the rotationally broadened line profile. In the present study, any rotational broadening is convolved with Stark broadening in the Balmer lines and is difficult to interpret. Consequently, whilst we suspect that there may be evidence for line-profile variations with similar frequencies to the radial motions, we can draw no firm conclusions from the present data.

Table 4. Velocity amplitudes of detected pulsation modes in PB 8783. Symbols are as in table 2 except that ν_p, a_p are from SDBV V. The identification marked (:) is tentative.

ν_p mHz	a_p mmi	ν_v mHz	a_v km s^{-1}
7.338	0.28	7.339	1.22
7.453	1.78]		
7.454	1.09]	7.456	1.54
7.870	1.62	7.857	1.23
8.090	1.20		
8.1507	2.09]		
8.1516	1.65]	8.141	1.91
8.1526	1.18]		
8.589	0.27	8.561:	1.09:
10.587	0.17]		
10.623	0.38]	10.625	2.18

3.3 PB 8783

The binary PB 8783 is altogether more difficult to analyze because of the superposition of sdB and F star spectra. The results shown in Fig. 3 are based on fitting parabola to $\chi(v)$ with $\delta v = 420 \text{ km s}^{-1}$. In deriving the amplitude spectrum in Fig. 3, the background function $b(t)$ was found to be best given by a sinusoid with an amplitude of 10 km s^{-1} , representing a systemic drift substantially larger than that in KPD 2109+4401.

On inspection, the typical ccf for PB 8783 consists of a strong broad component (FWHM $\sim 1400 \text{ km s}^{-1}$) superimposed by a small narrow component (FWHM $\sim 200 \text{ km s}^{-1}$, Fig. 4). The narrow feature disappears when the template is replaced by a theoretical sdB star spectrum containing H and He lines only, and is deduced to be due principally to metal-lines in the F-type secondary. This is confirmed when χ is calculated using only wavelengths between $H\delta$ and $H\gamma$; the broad component disappears leaving a small narrow peak.

The detection of two components in χ offers the possibility to resolve the radial motions of the binary components. The mutual motion of the F-star is clearly apparent when χ excludes the Balmer lines, and appears as a change of $\sim 10 \text{ km s}^{-1}$ during the five-hour observing run. However, the sign of the change remains the same when the theoretical sdB spectrum is used as a template, indicating that the Balmer lines in the F-star contribute significantly to χ .

The problem was resolved by fitting $\chi(-\delta v : +\delta v)$, $\delta v = 280 \text{ km s}^{-1}$ with the function $g(v) = g_0 \exp((v - g_1)^2/g_2) + g_3 + g_4v + g_5v^2$, where the quadratic terms fit the broad component and the gaussian terms represent the narrow component (Fig. 4). The functions $g_1(v)$ and $-g_4(v)/2g_5(v)$ were examined to determine the mutual motion of each star and to look for high-frequency content. The results are shown in Figs. 5 and 6 where it will be seen that the slowly varying components are of opposite sign. It is suggested that, in the absence of viable alternatives for these systematic drifts, these slowly varying components are most probably due to the mutual motion of the two stars within the binary.

If this is the case, a linear regression on the first 4 hours of both sets of velocity data gives the relative acceleration of the two components. The result, $\Delta v_F / \Delta v_{\text{sdb}} = -0.81 \pm 0.10$, provides an estimate for the mass ratio of the two stars

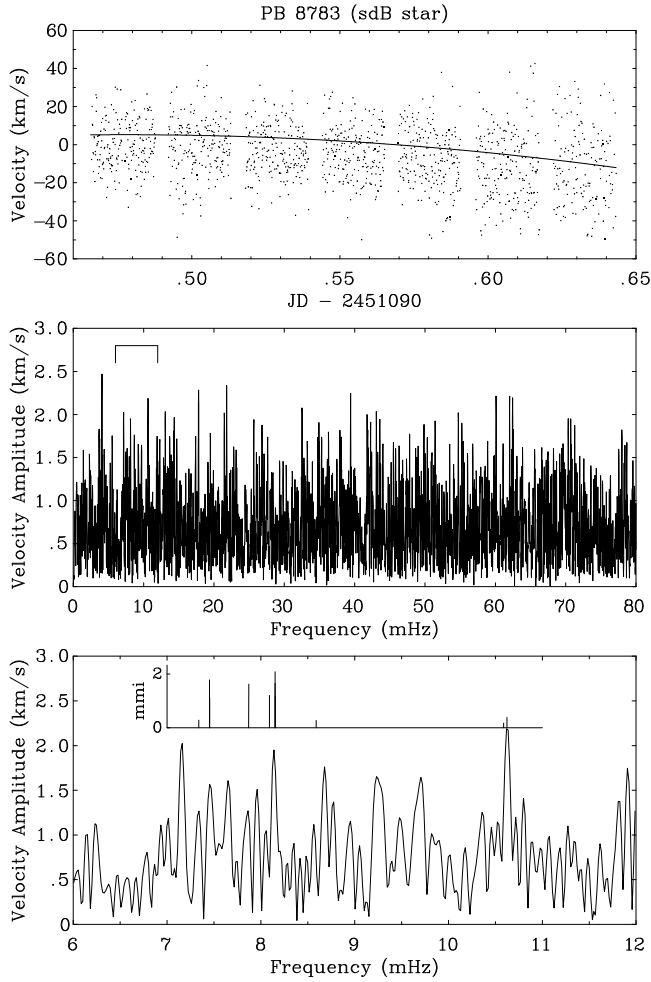


Figure 5. Radial velocities and amplitude spectrum of the sdB star in PB 8783. The least squares solution to the slowly varying velocity component is shown in the top panel (solid line). The amplitudes of photometric frequencies are as in Fig. 3.

$M_{\text{sdB}}/M_{\text{F}} \sim 0.8$. This is a little high for an F-star on the main-sequence ($1.1 - 1.8 M_{\odot}$) and a canonical sdB star ($\sim 0.5 M_{\odot}$), and suggests that the relative motions have still not been fully resolved. Further information concerning the velocities of the two components relative to one another is convolved into the composite Balmer profiles in the ccf template and will require observations of the complete binary orbit to disentangle. Whilst the binary period is clearly longer than the data sequence, it is constrained by the relation

$$K_{\text{F}} = 210 \frac{1}{1+q} \left(\frac{M}{P} \right)^{1/3} \sin i \text{ km s}^{-1}. \quad (1)$$

M is the total mass of the system (M_{\odot}), $q = M_{\text{F}}/M_{\text{sdB}}$ is the mass ratio, P is the orbital period (d) and K_{F} is the velocity semi-amplitude of the F star (km s^{-1}). For example, with $M_{\text{sdB}} = 0.55 M_{\odot}$, $M_{\text{F}} = 1.2 M_{\odot}$, $i = 30^{\circ}$ and $P = 2\text{d}$, $K_{\text{F}} = 32 \text{ km s}^{-1}$. The maximum change in velocity over the timescale of our observations (0.15d) would be $\Delta v_{\text{F}} \sim 15 \text{ km s}^{-1}$, compared with 13 km s^{-1} observed. Inverting the procedure, we can determine the maximum P as a function of i required to obtain $\Delta v_{\text{F}} = 13 \text{ km s}^{-1}$ in 0.15d. For $M_{\text{F}} = 1.2 - 1.8 M_{\odot}$, the maximum P increases from 1.0 – 0.8d at

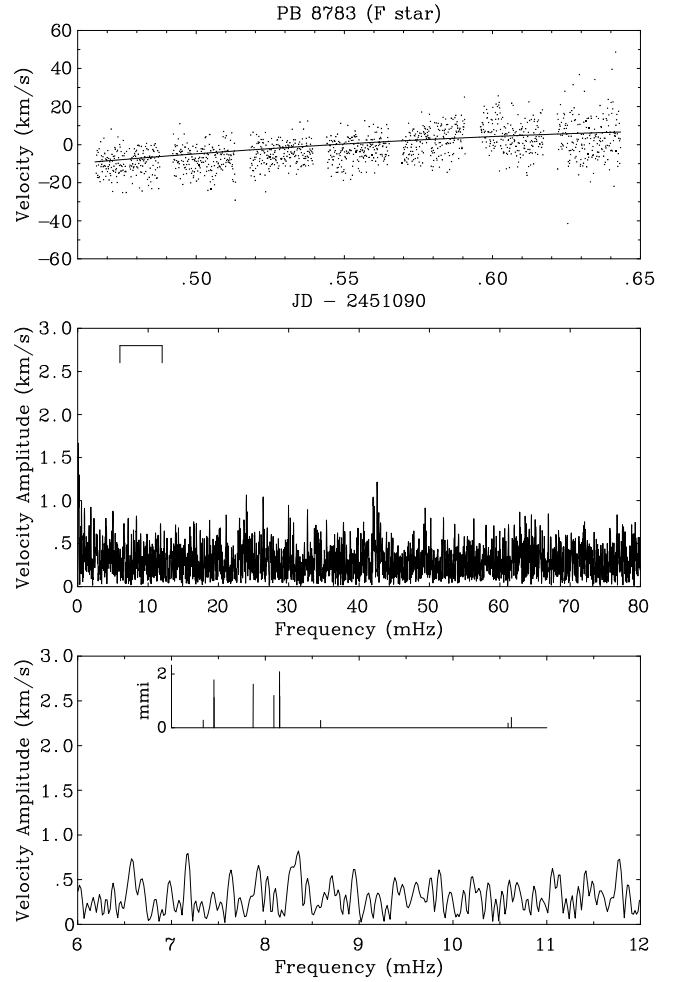


Figure 6. As Fig. 5 for the F star in PB 8783.

$i = 10^{\circ}$ to $P = 3.7 - 3.2\text{d}$ at $i = 80^{\circ}$. Eclipses are not expected at inclinations $\lesssim 80^{\circ}$.

It is satisfying to detect the photometric frequencies already reported for PB8783 (SDBV) in the deconvolved radial velocities of the sdB star (Fig. 5) and to find no such signal in the radial velocities of the F star (Fig. 6). This provides confirmation that the photometric and radial velocity variations are due to pulsations in the sdB star and not in the cool companion. A similar result was obtained for PG1336-018 (SDBV VIII), except in that case the persistence of oscillations during an eclipse of the unseen companion provided the necessary proof.

From this point, the interpretation of the sdB star velocities is the same as that for KPD2209+4101. Peaks in the velocity amplitude spectrum were identified at five frequencies also present in the photometry. The resulting pulsation velocity amplitudes were thus found to be in the range $1.1 - 2.2 \text{ km s}^{-1}$ and are shown in Table 4. Regarding the probability that these frequencies were identified by chance and following the prescription already given for KPD 2209+4101, we found with $v_{\text{thresh}} = 1.5 \text{ km s}^{-1}$ that $n = 9$, $n_{\text{id}} = 3$ and $p = 0.0034$ (Fig. 5). Relaxing $v_{\text{thresh}} = 1.0 \text{ km s}^{-1}$ yielded $n = 27$, $n_{\text{id}} = 6$ and $p = 0.0083$.

3.4 Relating luminosity and velocity amplitudes

Kjeldsen & Bedding (1995) investigated the relation between velocity and luminosity amplitudes for several classes of main-sequence, giant and supergiant pulsators and derived the calibrated relation

$$(\delta L/L)_\lambda = \frac{v_{osc}/\text{m s}^{-1}}{(\lambda/550\text{nm})(T_{\text{eff}}/5777\text{K})^2} 20.1\text{ppm}, \quad (2)$$

where ppm denotes parts-per-million.

We tested whether these predictions could be extended to the sdBVs since we have both light ($\delta L/L$) and velocity (v_{osc}) amplitudes for the same oscillation frequencies. We found that the observed velocity amplitudes are > 2 times those expected from the photometry and Eqn. (2). However Eqn. (2) has been derived from cool stars pulsating in radial or non-radial p-modes and it may not be applicable to pulsations in the hot sdBVs. We note that the amplitudes of individual modes in sdBVs have been reported to vary from one season and possibly one night to another (SDBV/VIII). Beating between unresolved modes will certainly affect the velocity amplitude measurements. Simultaneous high-speed photometry and spectroscopy will be required to properly relate the velocity and luminosity amplitudes and to make any further validation of Eqn. 2.

3.5 For future investigation

We have left two issues for future investigation.

1) Compared with its apparent surface gravity, the observed pulsation frequencies of PB 8783 are too high (SDBV XII). The expectation is that its surface gravity ($\log g = 5.55$, O'Donoghue et al. 1997, SDBV IV) should be much higher. It is recognised that this could be due to inadequate subtraction of the F-star spectrum, a conjecture which should be checked using higher quality data, including those presented here.

2) If the mode and amplitude of a spherical harmonic responsible for each pulsation frequency is specified, then it is relatively straightforward to integrate the projected surface velocities to provide a theoretical radial velocity curve. It is slightly more complicated to construct the theoretical light curve. From the combination it should be possible to refine the mode and amplitude measurements already established.

4 CONCLUSIONS

High-speed high-resolution spectroscopy of two non-radially pulsating subdwarf B stars KPD 2109+4401 and PB 8783 has been acquired with the William Herschel telescope. These data show radial velocity variations at both high- and low-frequencies. High-frequency peaks in the velocity amplitude spectrum correspond to frequencies identified in the light curves of both stars, and have allowed the velocity amplitudes associated with these stellar oscillations to be estimated. Typically $\sim 2\text{ km s}^{-1}$, these translate into radial variations of some 100–250 km within 60–90 s. The prospect for measuring the velocity amplitudes of non-radial pulsations in sdBVs with much higher amplitudes is promising. Line profile variations were not detected in the data although there are good reasons to suppose they should be present. The possibility that frequencies not present in the

photometry may contribute to the velocity amplitude spectrum should also be pursued.

In the case of the binary sdB PB 8783, low-frequency velocity variations corresponding to the mutual motion of both components have been resolved. These provide an upper limit to the orbital period of between 0.8 and 3 d, depending principally on the orbital inclination. Establishing the orbital period for this star should therefore be a priority for future observations. The deconvolution of component star velocities also demonstrated that high-frequency velocity variations occur only in the sdB star and not in the F star.

ACKNOWLEDGMENTS

This research has been supported by the Department of Education in Northern Ireland through a grant to the Armagh Observatory.

REFERENCES

- Benn C., 1997. "SIGNAL – exposure time calculator", Isaac Newton Group, La Palma
- Billères, Fontaine G., Brassard P., Charpinet S., Liebert J., Saffer R.A., Bergeron P., Vauclair G., 1998. ApJ 494, L75
- Billères, Fontaine G., Brassard P., Charpinet S., Liebert J., Saffer R.A., Vauclair G., 1998. ApJ 487, L81
- Charpinet S., Fontaine G., Brassard P., Chayer P., Rogers F.J., Iglesias C.A., Dorman B., 1997. ApJ 483, L123
- Kilkenny D., Koen C., O'Donoghue D., Stobie R.S., 1997. MNRAS 285, 640 (SDBV I)
- Kilkenny D., O'Donoghue D., Koen C., Lynas-Gray A.E., Van Wyk F., 1998. MNRAS 296, 329 (SDBV VIII)
- Kjeldsen H., Bedding T.R., 1995. A&A 293, 87
- Koen C., 1998. MNRAS 300, 567 (SDBV IX)
- Koen C., Kilkenny D., O'Donoghue D., Van Wyk F., Stobie R.S., 1997. MNRAS 285, 645 (SDBV II)
- Koen C., O'Donoghue D., Kilkenny D., Lynas-Gray A.E., Marang F., Van Wyk F., 1998a. MNRAS 296, 317 (SDBV VII)
- Koen C., O'Donoghue D., Pollacco D.L., Nitta A., Charpinet S., 1999. MNRAS 305, 28 (SDBV XII)
- O'Donoghue D., 1999. ASP Conf. Series 169, p.149.
- O'Donoghue D., Koen C., Solheim J.-E., Barstow M.A., Dobbie P.D., O'Brien M.S., Clemens J.C., Sullivan D.J., Kawaler S.D., 1998b. MNRAS 296, 296 (SDBV V)
- O'Donoghue D., Lynas-Gray A.E., Kilkenny D., Stobie R.S., Koen C., 1997. MNRAS 285, 657 (SDBV IV)
- O'Toole S.J., Teixeira T.C., Bedding T.R., Kjeldsen H., 2000. 'The Impact of Large-Scale Surveys on Pulsating Star Research', IAU Coll. 176, ASP Conf. Ser., L.Szabados, D.W.Kurtz, eds. (in press).
- Reid A., Bolton C.T., Crowe R.A., Fieldus M.S., Fullerton A.W., Gies D.R., Howarth I.D., McDavid D., Prinja R.K., Smith K.C., 1993. ApJ 417, 320
- Rutten R., Gribbin F., Ives D., Bennett T., Dhillon V., 1997. "Drift-Mode CCD readout - User's Manual", Isaac Newton Group, La Palma
- Telting J.H., Aerts C., Mathias P., 1997. A&A 322, 493